PAPER

Check for updates

A tetracyclic-bislactone-based copolymer donor for efficient semitransparent organic photovoltaics†

Mingjie Li,‡[ab] Tai An,‡[bc] Zongliang Ou,[bd] Ke Jin,[bc] Zhiwen Jin, [ID][e] Keyou Yan, [ID][f] He Tian, [ID][g] Wentao Wang,[h] Shangfeng Yang, [ID][i] Guan-Wu Wang, [ID]*[a] Qiuling Song,*[d] Zuo Xiao [ID]*[bc] and Liming Ding [ID][bc]

A copolymer donor PBDTTPTP based on a tetracyclic bislactone unit, thieno[2′,3′:5,6]pyrano[3,4-*d*]thieno[3,2-*b*]pyran-4,9-dione (TPTP), was developed. The single crystal structure of a TPTP derivative indicates the π-extended planar geometry of TPTP and its good coplanarity with the adjacent thiophene units. Thanks to the strong electron-withdrawing properties and good coplanarity of TPTP, the copolymer PBDTTPTP shows a deep HOMO level of −5.60 eV, a small optical bandgap of 1.65 eV and a good hole mobility of 6.57×10^{-4} cm^2 V^{-1} s^{-1}. These features make PBDTTPTP an efficient donor material for semitransparent organic photovoltaics (STOPVs). STOPVs based on PBDTTPTP and N3 gave a high light utilization efficiency of 4.38%, with a power conversion efficiency of 12.26% and an average visible light transmittance of 35.7%.

Introduction

Semitransparent photovoltaics (STPVs) with balanced energy-harvesting functionality and aesthetics show promise for architecture applications, such as power generating windows, curtains, and rooftops.[1–5] Power conversion efficiency (PCE) is no longer the only performance criterion. An ideal STPV should allow as much visible photons to pass through as possible to achieve a high average visible light transmittance (AVT), and should effectively convert non-visible photons into electricity to achieve a high PCE.[6–9] In this regard, the light utilization efficiency (LUE) (LUE = PCE × AVT) has been suggested as a figure of merit for STPVs.[10,11] As the human eyes are mainly sensitive to light at 400–700 nm,[12] it is wise to develop STPVs that selectively harvest the near-infrared (NIR) photons.[13–16] Organic photovoltaics (OPVs) can meet such requirements since organic semiconductors generally show a band-like absorption spectrum and it is easy to adjust their absorption bands in the NIR region.[17–20] In recent years, the development of low-bandgap small molecule acceptors (SMAs) has greatly accelerated the advancement of OPVs. Single-junction OPVs based on a wide-bandgap polymer donor and a low-bandgap SMA can afford >19% PCEs.[21–30] However, for semitransparent OPVs (STOPVs) the use of wide-bandgap donors is not a good choice since the donors absorb considerable visible light and reduce the AVT.[15,31–33] The development of efficient low-bandgap or mid-bandgap donors is crucial for high-performance STOPVs.

In 2012, Yang *et al.* first reported the diketopyrrolopyrrole based low-bandgap copolymer PBDTT-DPP for STOPVs (Fig. 1).[34,35] PBDTT-DPP shows an optical bandgap (E_g^{opt}) of 1.46 eV. STOPVs based on PBDTT-DPP and PC$_{71}$BM gave a PCE of 4.0% and an AVT of 61%, yielding a LUE of 2.44%. Later, Jen *et al.* developed a fused-quinoxaline based copolymer PIDT-PhanQ (E_g^{opt} of 1.67 eV) for STOPVs.[36] The semitransparent devices showed a LUE of 1.34%, with a PCE of 4.2% and an AVT of 32%. By using a

[a] Hefei National Research Center for Physical Sciences at the Microscale, University of Science and Technology of China, Hefei 230026, China.
E-mail: gwang@ustc.edu.cn

[b] Center for Excellence in Nanoscience, Key Laboratory of Nanosystem and Hierarchical Fabrication (CAS), National Center for Nanoscience and Technology, Beijing 100190, China. E-mail: xiaoz@nanoctr.cn

[c] University of Chinese Academy of Sciences, Beijing 100049, China

[d] Institute of Next Generation Matter Transformation, College of Materials Science & Engineering, Huaqiao University, Xiamen 361021, China.
E-mail: qsong@hqu.edu.cn

[e] School of Physical Science and Technology, Lanzhou University, Lanzhou 730000, China

[f] School of Environment and Energy, South China University of Technology, Guangzhou 510000, China

[g] School of Integrated Circuits, Tsinghua University, Beijing 100084, China

[h] School of Materials Science and Engineering, Zhejiang Sci-Tech University, Hangzhou 310018, China

[i] Department of Materials Science and Engineering, University of Science and Technology of China, Hefei 230026, China

† Electronic supplementary information (ESI) available. CCDC 2167880. For ESI and crystallographic data in CIF or other electronic format see DOI: https://doi.org/10.1039/d3ma00179b

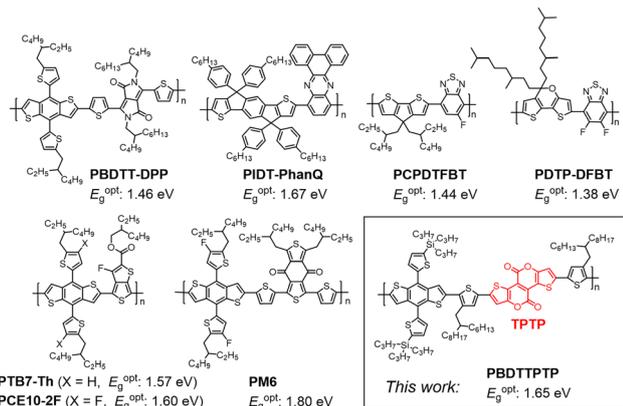‡ M. Li and T. An contributed equally to this work.

Fig. 1 Previous low-bandgap and mid-bandgap copolymer donors and PBDTTPTP in this work for STOPVs.

benzothiadiazole based copolymer PCPDTFBT with a smaller E_g^{opt} of 1.44 eV, Jen *et al.* achieved a higher LUE of 2.37%, with a PCE of 5.0% and an AVT of 47.3%.[37] The benzothiadiazole copolymer PDTP-DFBT developed by Yang *et al.* shows a very small E_g^{opt} of 1.38 eV.[38] By blending PDTP-DFBT with a low-bandgap acceptor FOIC, Sun *et al.* made STOPVs with a LUE of 2.15%, a PCE of 3.5% and an AVT of 61.5%.[39] PTB7-Th is a classic low-bandgap copolymer with an E_g^{opt} of 1.57 eV.[40,41] By combining PTB7-Th with two low-bandgap acceptors CO$_i$8DFIC and IEICO-4F, Zhang *et al.* achieved a LUE of 1.71% for semitransparent solar cells.[42] Zhu *et al.* improved the LUE to 3.33% by blending PTB7-Th with another acceptor ATT-9.[43] By using an outcoupling layer, an antireflection layer and a low-bandgap acceptor A078, Forrest *et al.* achieved a remarkable LUE of 5.0% for PTB7-Th-based STOPVs.[44] Very recently, Chen *et al.* achieved a high LUE of 5.01% by using PCE10-2F (a congener of PTB7-Th) as the donor and Y6 as the acceptor *via* a sequential deposition technique.[45] PM6 is a highly efficient mid-bandgap copolymer donor for both opaque and semitransparent OPVs.[46] By introducing a small molecule 2PACz into the PM6:Y6-BO blend, Huang *et al.* realized a LUE of 3.39% for semitransparent devices.[47] Chen *et al.* demonstrated high-performance STOPVs with a LUE of 5.0% based on PM6 and two Y-series acceptors, BTP-eC9 and L8-BO.[48] By integrating an aperiodic band-pass filter (ABPF), Li *et al.* achieved a LUE of 5.35%, with a PCE of 11.44% and an AVT of 46.79%.[49] The 5.35% LUE is the highest value for STOPVs to date.

Despite the progress mentioned above, there is still plenty of room for designing new and efficient low-bandgap or mid-bandgap copolymers for STOPVs. Previously, our group demonstrated that fused-ring aromatic lactones (FRAL) are efficient building blocks for high-performance copolymer donors.[50–57] In this work, we report the synthesis of a copolymer donor PBDTTPTP by using a novel tetracyclic bislactone unit, thieno[2′,3′:5,6]pyrano[3,4-*d*]thieno[3,2-*b*]pyran-4,9-dione (TPTP). Thanks to the strong electron-withdrawing properties and good coplanarity of TPTP, PBDTTPTP shows a relatively small E_g^{opt} of 1.65 eV, a deep HOMO level and good hole mobility, and exhibits good performance in STOPVs. An impressive LUE of 4.38% was achieved by the STOPVs based on PBDTTPTP and a low-bandgap acceptor N3.[58]

Results and discussion

The synthesis of PBDTTPTP is shown in Fig. 2a. Synthetic details are provided in the ESI.† 3-Thiophene boric acid was oxidized by hydrogen peroxide to give the intermediate 3-hydroxythiophene. Then, the hydroxyl group of 3-hydroxythiophene was quickly protected by the methoxymethyl (MOM) group, affording compound **1** in 65% yield. Compound **1** was transformed into the organotin compound **2** in 43% yield. Stille coupling of **2** and dimethyl 2,3-dibromobut-2-enedicarboxylate gave compound **3** in 72% yield. Two stages of bromination transformed compound **3** to compound **4** in 74% yield. Treating **4** with *p*-toluenesulfonic acid gave the brominated tetracyclic bislactone TPTP-Br in 77% yield. It should be noted that compounds **1–4** with MOM groups are not stable, especially in solution. Therefore, they should be quickly used for the next reaction step. TPTP-Br further underwent Stille coupling with tributyl(4-(2-butyloctyl)thiophen-2-yl)stannane or tributyl(4-(2-hexyldecyl)thiophen-2-yl)stannane to give compound **5** or **6** in 86% or 85% yield, respectively. Treating compound **5** or **6** with *N*-bromosuccinimide afforded compound **7** or **8** in 98% yield. Finally, Stille copolymerization of **8** and (2,6-bis(trimethylstannyl)benzo[1,2-*b*:4,5-*b′*]dithiophene-4,8-diyl)bis(thiophene-5,2-diyl))bis(tripropylsilane) (BDT-Si-Sn) gave the copolymer donor PBDTTPTP in 67% yield. The number-average molecular weight (M_n) and polydispersity index (PDI) for PBDTTPTP are 51.6 kDa and 1.80, respectively. PBDTTPTP shows good solubility in chloroform and chlorobenzene. We tried the copolymerization of **7** and BDT-Si-Sn (Scheme S1, ESI†). However, the resulting copolymer is insoluble, probably due to the shorter 2-butyloctyl side chains on the thiophene bridges. We also tried the copolymerization of **8** with other BDT donor units, (4,8-bis(5-(2-ethylhexyl)-4-fluorothiophen-2-yl)benzo[1,2-*b*:4,5-*b′*]dithiophene-2,6-diyl)bis(trimethylstannane) (BDT-F-Sn) and (4,8-bis(5-(2-ethylhexyl)-4-chlorothiophen-2-yl)benzo[1,2-*b*:4,5-*b′*]dithiophene-2,6-diyl)-bis(trimethylstannane) (BDT-Cl-Sn). But these copolymers are also insoluble in common organic solvents (Scheme S1, ESI†). These results indicate that the bulky tripropylsilyl side chains on BDT units and the long 2-hexyldecyl side chains on the thiophene bridges are crucial for providing sufficient solubility for the copolymer. The synthetic complexity (SC)[59,60] of PBDTTPTP was analysed (Table S1, ESI†). Compared with other reported polymers shown in Fig. 1, PBDTTPTP shows a moderate SC of 66.91%. All new compounds were characterized by spectroscopic methods like NMR and mass spectroscopy. The characterization data are consistent with the molecular structures shown in Fig. 2. The structure of compound **7** was unambiguously determined by single crystal X-ray diffraction (XRD) analysis (Fig. 2b). The top-view confirms the linear and π-extended molecular geometry of the TPTP unit. The side-view indicates the good coplanarity between the thiophene bridge and TPTP. Interestingly, the thiophene bridge and the thiophene ring of TPTP adopt a *cis* arrangement. The molecular packing indicates the efficient π–π stacking of **7** in the crystal. Due to the extended molecular plane of TPTP and the good coplanarity, compound **7** shows a short average π–π stacking distance of 3.54 Å. Efficient π–π stacking would enhance the crystallinity and charge carrier mobility of the copolymer
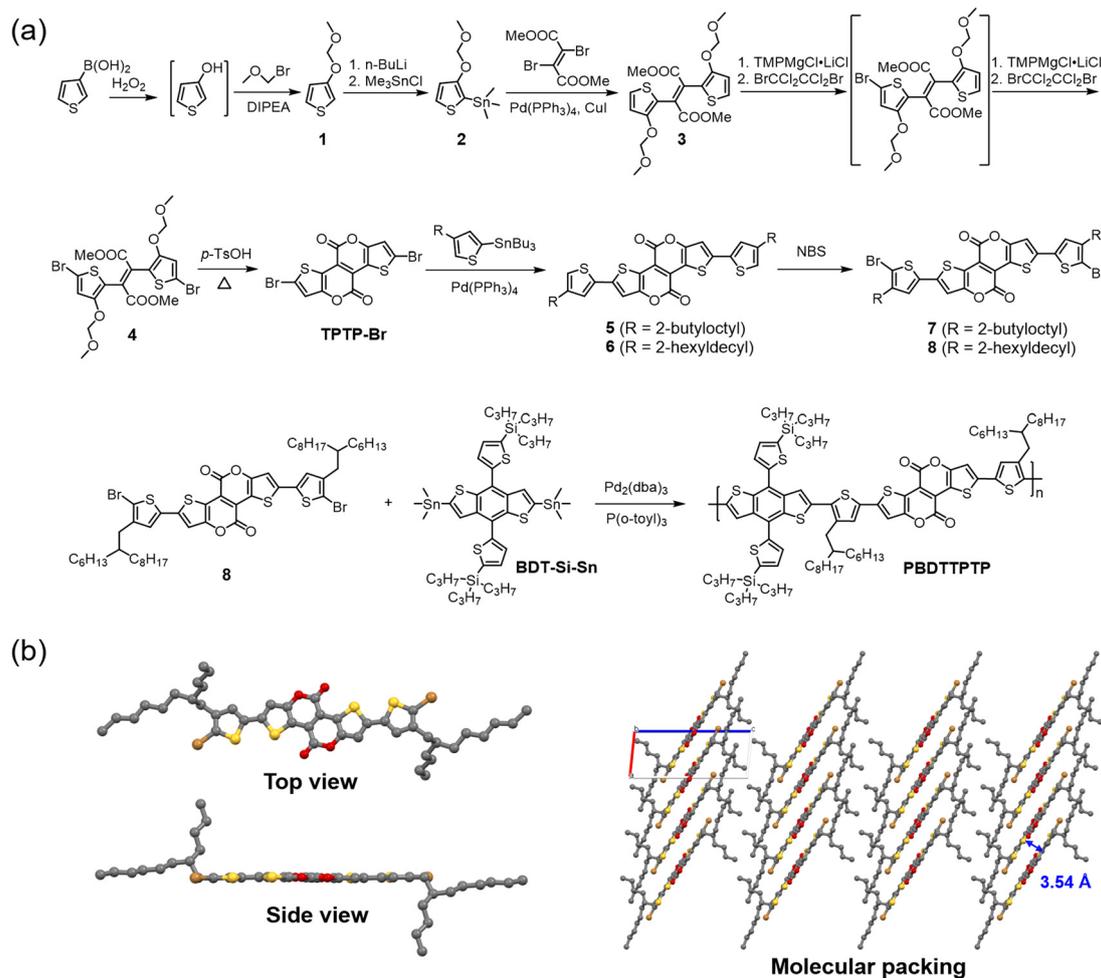
Fig. 2 (a) Synthetic route for PBDTTPTP; (b) the top view, side view and molecular packing (viewing along the *b*-axis) of the single crystal structure of compound **7**.

PBDTTPTP. We measured the hole mobility (μ_h) of PBDTTPTP by using the space charge limited current (SCLC) method (Fig.

Fig. 3 (a) Absorption spectra of PBDTTPTP in solution and film states and N3 film. (b) Energy level diagram. (c) The chemical structure of N3 and the conventional device structure.

S15, ESI†).[61–63] The copolymer shows a good μ_h of 6.57×10^{-4} cm^2 V^{-1} s^{-1}.

The optical and electrochemical properties of PBDTTPTP were investigated (Fig. 3). In solution, PBDTTPTP presents a major absorption band in the range of 520–750 nm, with a peak at 683 nm and a shoulder peak at 654 nm. In the film state, these two peaks shift to 688 nm and 636 nm, respectively. The absorption onset of the PBDTTPTP film is at 752 nm, corresponding to a small E_g^opt of 1.65 eV. The HOMO and the lowest unoccupied molecular orbital (LUMO) energy levels were estimated from cyclic voltammetry (CV) measurements (Fig. S16, ESI†).[64] The PBDTTPTP film shows an onset oxidation potential of 0.80 V and an onset reduction potential of −1.69 V, respectively, corresponding to the HOMO level of −5.60 eV and LUMO level of −3.11 eV, respectively. Such a deep HOMO level of PBDTTPTP is favorable for high open-circuit voltages (V_oc) in solar cells.

Before application in STOPVs, we evaluated the performance of PBDTTPTP in opaque solar cells with a conventional device structure of glass/ITO/PEDOT:PSS/PBDTTPTP:N3/PDIN/Ag (80 nm). The active layer thickness (Table S2, ESI†) and the D/A ratio (Fig. 4a and Table 1) were optimized. It was found that when the active
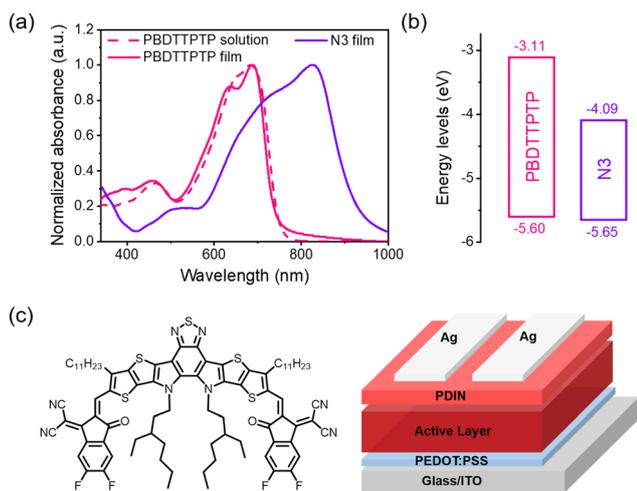
layer thickness is 128 nm and the D/A ratio is 1:1.4, the opaque devices gave the best PCE of 15.28%, with a V_{oc} of 0.829 V, a short-circuit current density (J_{sc}) of 25.43 mA cm^{-2} and a fill factor (FF) of 72.5%. The cells showed over 70% external quantum efficiency (EQE) in the 430–842 nm region, with a maximum EQE of 78.5% at 750 nm (Fig. 4b). For STOPV development, a common strategy is reducing the donor content in the active layer to enhance the visible transmittance.[19,65,66] Therefore, efficient low-donor-content cells are favorable for STOPVs. We found that the PBDTTPTP:N3 cells can maintain decent PCEs even with a very low donor content. When the D/A ratio is 1:2.6 or 1:3.2, the cells still afforded good PCEs of 13.11% and 11.76%, respectively (Table 1). For these low-donor-content cells, decent FFs of over 70% were achieved, suggesting that the charge carrier transport is still efficient in these cells. SCLC measurements indicate that the D/A ratio variation has insignificant effects on charge carrier mobilities (Fig. 4c). When the D/A ratio changed from 1:1.2 to 1:3.2, μ_h decreased from 6.80×10^{-4} to 5.94×10^{-4} cm^2 V^{-1} s^{-1} and the electron mobility (μ_e) increased from 4.46×10^{-4} to 5.85×10^{-4} cm^2 V^{-1} s^{-1} (Fig. S19, S20 and Table S3, ESI†). In low-donor-content cells, the active layer kept its efficient and balanced hole and electron transport capability, thus showing high FF. To understand the robust charge transport capability of the PBDTTPTP:N3 layer, we studied the film morphology at different D/A ratios (1:1.4, 1:2.0 and 1:2.6) by employing an atomic force microscope (AFM).[67] All films show similar morphology with a nanofibrillar texture (Fig. S21, ESI†), suggesting that the donor–acceptor phase segregation is less

Table 1 The performance of PBDTTPTP:N3 opaque solar cells[a]

D:A [w:w]	V_{oc} [V]	J_{sc} [mA cm^{-2}]	FF [%]	PCE [%]
1:1.2	0.816	24.77	69.1	13.95 (13.71)[b]
1:1.4	0.829	25.43	72.5	15.28 (15.17)
1:1.6	0.829	24.41	71.0	14.38 (14.22)
1:2.0	0.830	23.03	71.0	13.56 (13.41)
1:2.6	0.835	21.88	71.8	13.11 (13.00)
1:3.2	0.844	19.90	70.0	11.76 (11.43)

[a] Device structure: glass/ITO/PEDOT:PSS/PBDTTPTP:N3/PDIN/Ag (80 nm). [b] Data in parentheses stand for the average PCEs for 10 cells.

affected by the D/A ratio in PBDTTPTP:N3 cells. The V_{oc} increases along with the N3 content. It could be due to the decrease in the energy loss (E_{loss}) of the cells as the nonfullerene acceptor content increases.[68–71] The absorption spectra (normalized at 817 nm) of the active layer with different D/A ratios are shown in Fig. 4d. The films with a lower donor content show much reduced absorbance in the visible region, which might be favorable for STOPV development. It should be noted that the shape of the EQE spectra of the low-donor-content cells did not change much as compared to those of the high-donor-content cells. This suggests that the photon-to-electron conversion in the visible region could be more efficient than that in the NIR region for the low-donor-content cells.

The charge recombination and collection in PBDTTPTP:N3 cells were investigated. Charge recombination was studied by plotting V_{oc} against light intensity (P_{light}) (Fig. S22, ESI†). The slope can be expressed as nk_BT/q, where k_B is the Boltzmann
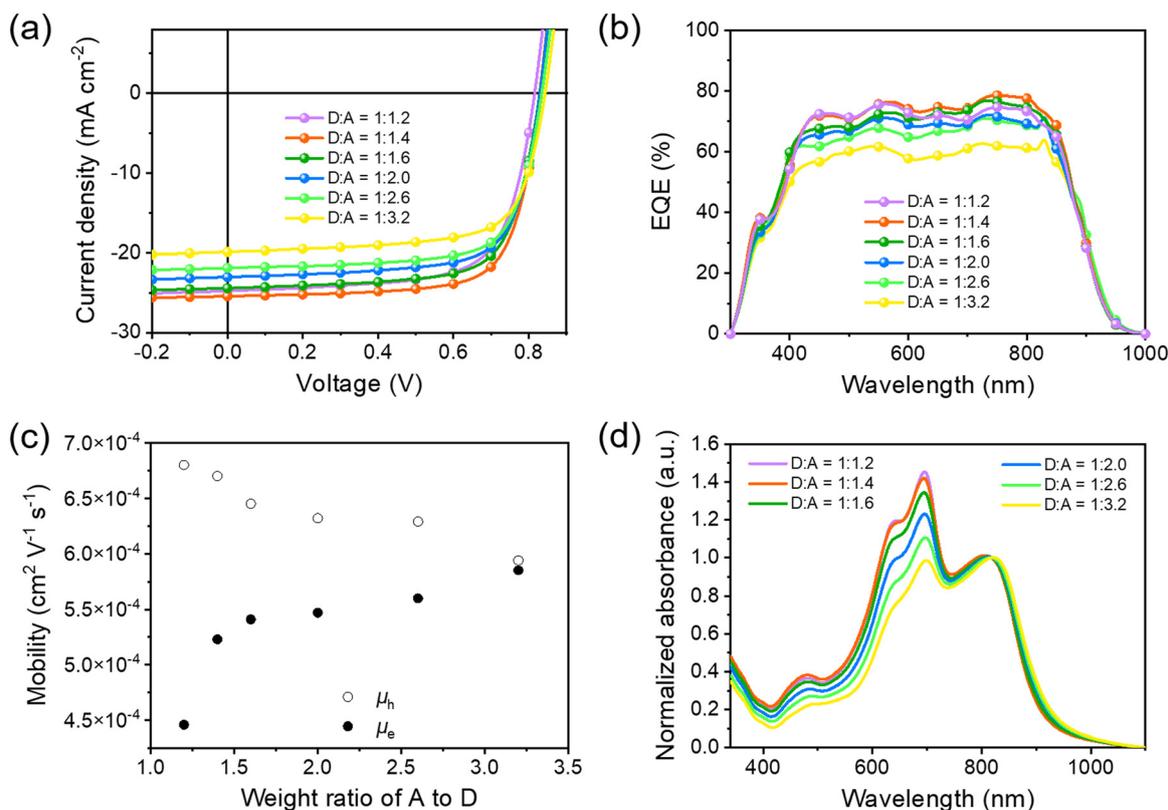

Fig. 4 (a) J–V curves of PBDTTPTP:N3 opaque solar cells with different D/A ratios. (b) EQE spectra. (c) The variation of μ_h and μ_e along with the A/D ratio. (d) Absorption spectra (normalized at 817 nm) of the active layer with different D/A ratios.

constant, T is the absolute temperature and q is the elemental charge. When n is close to 1, bimolecular recombination is dominant. When n is close to 2, trap-assisted charge recombination is dominant. We found that the slopes for varied D/A ratios are always closer to 1, suggesting that bimolecular recombination is the dominant charge recombination pathway for these systems. Then, the bimolecular recombination was studied by plotting J_{sc} against light intensity (P_{light}) (Fig. S23, ESI†). The exponent α reflects the degree of bimolecular recombination ($\alpha = 1$ manifests no bimolecular recombination). Among the solar cells, the devices with the D/A ratio of 1:1.4 show an α of 0.982 (the closest value to 1), suggesting the minimum bimolecular recombination in these cells. We further analysed the exciton dissociation probabilities (P_{diss}) and charge collection probabilities (P_{coll}) by plotting the photocurrent density (J_{ph}) against effective voltage (V_{eff}) for the solar cells with different D/A ratios (Fig. S24, ESI†). It was found that the cells with the ratio of 1:1.4 gave highest P_{diss} of 97.1% and highest P_{coll} of 87.9%, suggesting the most efficient charge generation and collection. The above results are consistent with the highest J_{sc} of the PBDTTPTP:N3 (1:1.4) solar cells.

Next, we fabricated STOPVs by replacing the opaque thick Ag electrode (80 nm) with a semitransparent thin Au/Ag electrode.[68,72] The thicknesses of Au and Ag were optimized. When using 1 nm-thick Au and 15 nm-thick Ag as the electrode, the STOPV gave the most balanced PCE and AVT (Tables S4, S5 and

Fig. S25, S26, ESI†). According to the literature, the Au (1 nm) seed layer could improve the conductivity thus enhancing the J_{sc} of semitransparent devices.[73,74] The J–V curves and device performance data for semitransparent cells with different D/A ratios are shown in Fig. 5a and Table 2, respectively. The EQE spectra are shown in Fig. S28 (ESI†). The variation trend of PCE along with D/A ratios was similar to that in opaque cells. Thus, the cells with a D/A ratio of 1:1.4 afforded the highest PCE of 13.61%. However, these cells showed a relatively low AVT of 18.4%, thus giving a moderate LUE of 2.50%. As the donor content in the active layer gradually decreases, the PCE slightly decreases while the AVT continuously increases, leading to the increment in LUE. When the D/A ratio is 1:2.6, the semitransparent cells gave the highest LUE of 2.88%, with a PCE of 12.61% and an AVT of 22.8%. We also tried to combine PBDTTPTP with other low-bandgap acceptors like Y6 and BTP-eC9 (Table S7 and Fig. S29, ESI†). Under the same conditions, although PBDTTPTP:Y6 and PBDTTPTP:BTP-eC9 semitransparent cells achieved higher V_{oc}, their J_{sc}, FF and AVT are lower than those of PBDTTPTP:N3 semitransparent cells, leading to reduced PCEs and LUEs. The light-soaking stability of the opaque and semitransparent PBDTTPTP:N3 cells was investigated (Fig. S30, ESI†). Continuously illuminating opaque and semitransparent cells (with a D/A ratio of 1:2.6) with a Xenon lamp (AM 1.5G, 1 sun irradiation) for 20 hours, the PCEs dropped to 27% and 31% of the initial values for opaque and
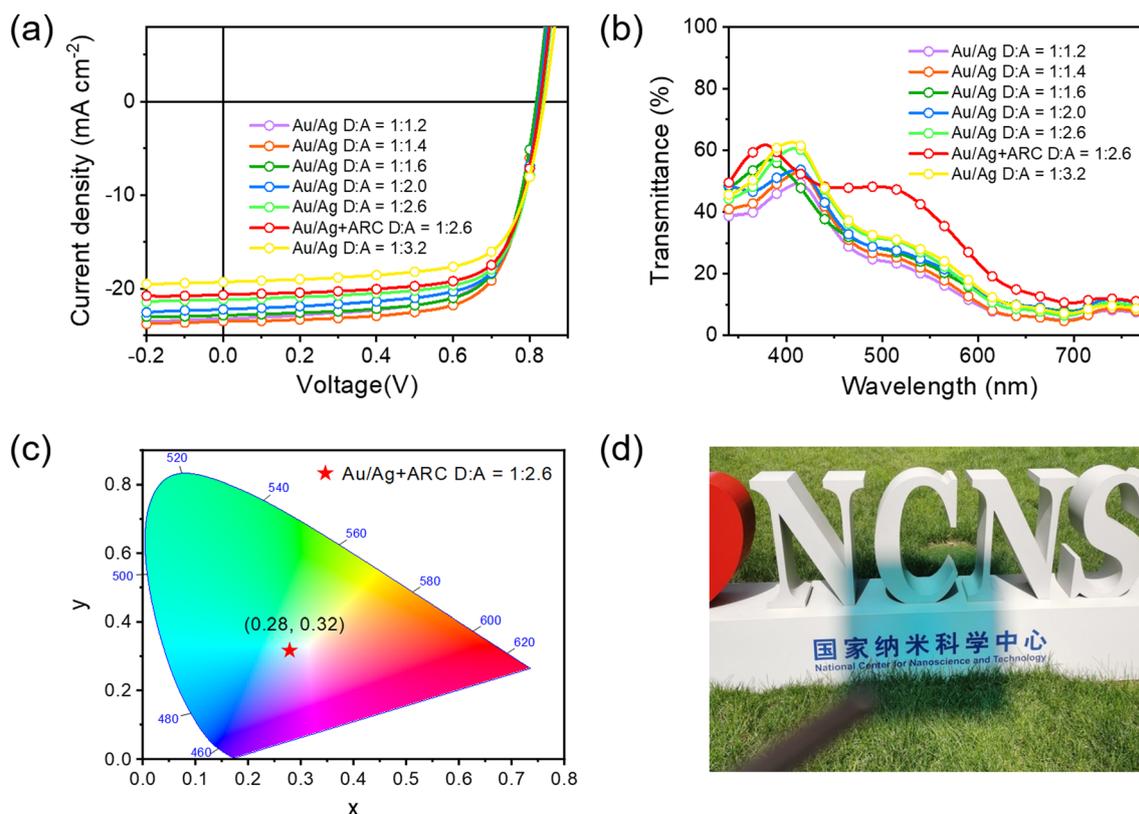

Fig. 5 (a) J–V curves of PBDTTPTP:N3 semitransparent solar cells with different D/A ratios. (b) Transmittance spectra. (c) Coordinates of CIE 1931 for the best-LUE cell. (d) The photograph of a 1 cm^2 semitrasparent cell made under optimal conditions.

Table 2 The performance of PBDTTPTP:N3 semitransparent solar cells[a]

D:A [w:w]	V_{oc} [V]	J_{sc} [mA cm^{-2}]	FF [%]	PCE [%]	AVT [%]	LUE [%]
1:1.2	0.817	23.21	68.9	13.05 (13.00)[b]	16.9	2.21
1:1.4	0.821	23.47	70.6	13.61 (13.46)	18.4	2.50
1:1.6	0.818	22.83	70.5	13.17 (12.61)	20.8	2.74
1:2.0	0.824	22.20	70.5	12.91 (12.48)	21.6	2.79
1:2.6	0.831	21.14	71.8	12.61 (12.21)	22.8	2.88
1:2.6[c]	0.828	20.65	71.7	12.26 (12.17)	35.7	4.38
1:3.2	0.838	19.28	69.6	11.25 (10.83)	24.0	2.70

[a] Device structure: glass/ITO/PEDOT:PSS/PBDTTPTP:N3/PDIN/Au (1 nm)/Ag (15 nm). [b] Data in parentheses stand for the average PCEs for 10 cells. [c] Device structure: MgF$_2$ (100 nm)/glass/ITO/PEDOT:PSS/PBDTTPTP:N3/PDIN/Au (1 nm)/Ag (15 nm)/MoO$_3$ (35 nm).

semitransparent cells, respectively. It can be concluded that these cells are not so stable under continuous illumination.

To further improve the LUE of PBDTTPTP:N3 semitransparent cells, we used antireflective coating (ARC) to enhance the AVT of the whole device. Thus, MgF$_2$ (100 nm) and MoO$_3$ (35 nm) were employed as ARC to reduce the reflection at the ITO side and the Ag side, respectively.[75] With MgF$_2$ as the sole ARC, the AVT increased from 22.8% to 26.7%, leading to an enhanced LUE of 3.33% (Fig. S27 and Table S6, ESI†). With both MgF$_2$ and MoO$_3$ ARC, the transmittance at 450–700 nm was largely enhanced (Fig. 5b). The AVT increased to 35.7% and the LUE increased to 4.38% for the best semitransparent cells. To our knowledge, the 4.38% LUE is among the highest values for STOPVs to date. The aesthetic aspect is also an important criterion for STOPVs. The transmitted light should have a chromaticity close to that of the natural white light source for a harmonious visual environment and comfort. According to the chromaticity diagram released by Commission Internationale de l'Eclairage (CIE) in 1931, chromaticity coordinates of white light are (0.33, 0.33). We measured the color coordinates of our best-LUE cells. As shown in Fig. 5c, the coordinates are (0.28, 0.32), which are close to that of the white light and suggest the good color rendering properties of these devices. The measured color rendering index (CRI) of the best-LUE cells is 91.[76–78] The high LUE together with the good color rendering properties of the semitransparent cells suggest their potential in power generating windows. Fig. 5d shows the photograph of a 1 cm^2 semitransparent cell made under optimal conditions. The background can be seen clearly. The 1 cm^2 semitransparent cell gave a slightly reduced PCE of 11.40% (Table S8 and Fig. S31, ESI†).

Conclusions

To conclude, by using a tetracyclic bislactone unit TPTP, we developed an efficient copolymer donor PBDTTPTP for STOPVs. The strong electron-withdrawing properties and good coplanarity of TPTP endow PBDTTPTP with a small E_g^{opt} of 1.65 eV, a deep HOMO level and good hole mobility. PBDTTPTP not only delivered a decent PCE of 15.28% in opaque solar cells, but also achieved a high LUE of 4.38% (a PCE of 12.26% and an AVT of 35.7%) in STOPVs. This work suggests that FRAL units are

promising building blocks for low-bandgap copolymer donors for STOPVs.

Conflicts of interest

There are no conflicts to declare.

Acknowledgements

References

1 Y. Li, G. Xu, C. Cui and Y. Li, *Adv. Energy Mater.*, 2018, **8**, 1701791.

2 Y. Liu, P. Cheng, T. Li, R. Wang, Y. Li, S.-Y. Chang, Y. Zhu, H.-W. Cheng, K.-H. Wei, X. Zhan, B. Sun and Y. Yang, *ACS Nano*, 2019, **13**, 1071–1077.

3 D. Wang, H. Liu, Y. Li, G. Zhou, L. Zhan, H. Zhu, X. Lu, H. Chen and C.-Z. Li, *Joule*, 2021, **5**, 945–957.

4 W. Li, C. Lin, G. Huang, J. Hur, B. Huang and S. Yao, *Adv. Sci.*, 2022, **9**, 2201738.

5 D. Wang, Y. Li, G. Zhou, E. Gu, R. Xia, B. Yan, J. Yao, H. Zhu, X. Lu, H.-L. Yip, H. Chen and C.-Z. Li, *Energy Environ. Sci.*, 2022, **15**, 2629–2637.

6 V. V. Brus, J. Lee, B. R. Luginbuhl, S.-J. Ko, G. C. Bazan and T.-Q. Nguyen, *Adv. Mater.*, 2019, **31**, 1900904.

7 T. Jiang, G. Zhang, R. Xia, J. Huang, X. Li, M. Wang, H.-L. Yip and Y. Cao, *Mater. Today Energy*, 2021, **21**, 100807.

8 C. Xu, K. Jin, Z. Xiao, Z. Zhao, Y. Yan, X. Zhu, X. Li, Z. Zhou, S. Y. Jeong, L. Ding, H. Y. Woo, G. Yuan and F. Zhang, *Sol. RRL*, 2022, **6**, 2200308.

9 T. Xu, Y. Luo, S. Wu, B. Deng, S. Chen, Y. Zhong, S. Wang, G. Lévêque, R. Bachelot and F. Zhu, *Adv. Sci.*, 2022, **9**, 2202150.

10 C. J. Traverse, R. Pandey, M. C. Barr and R. R. Lunt, *Nat. Energy*, 2017, **2**, 849–860.

11 C. Yang, D. Liu, M. Bates, M. C. Barr and R. R. Lunt, *Joule*, 2019, **3**, 1803–1809.

12 Q. Xue, R. Xia, C. J. Brabec and H.-L. Yip, *Energy Environ. Sci.*, 2018, **11**, 1688–1709.

13 R. R. Lunt and V. Bulovic, *Appl. Phys. Lett.*, 2011, **98**, 113305.

14 Y. Li, J.-D. Lin, X. Che, Y. Qu, F. Liu, L.-S. Liao and S. R. Forrest, *J. Am. Chem. Soc.*, 2017, **139**, 17114–17119.

15 X. Huang, J. Oh, Y. Cheng, B. Huang, S. Ding, Q. He, F. Wu, C. Yang, L. Chen and Y. Chen, *J. Mater. Chem. A*, 2021, **9**, 5711–5719.

16 W. Liu, S. Sun, L. Zhou, Y. Cui, W. Zhang, J. Hou, F. Liu, S. Xu and X. Zhu, *Angew. Chem., Int. Ed.*, 2022, **61**, e202116111.

17 A. Polman, M. Knight, E. C. Garnett, B. Ehrler and W. C. Sinke, *Science*, 2016, **352**, aad4424.

18 W. Wang, C. Yan, T.-K. Lau, J. Wang, K. Liu, Y. Fan, X. Lu and X. Zhan, *Adv. Mater.*, 2017, **29**, 1701308.

19 Y. Xie, Y. Cai, L. Zhu, R. Xia, L. Ye, X. Feng, H.-L. Yip, F. Liu, G. Lu, S. Tan and Y. Sun, *Adv. Funct. Mater.*, 2020, **30**, 2002181.

20 N. Schopp and V. V. Brus, *Energies*, 2022, **15**, 4639.

21 K. Jin, Z. Xiao and L. Ding, *J. Semicond.*, 2021, **42**, 060502.

22 X. Meng, K. Jin, Z. Xiao and L. Ding, *J. Semicond.*, 2021, **42**, 100501.

23 K. Chong, X. Xu, H. Meng, J. Xue, L. Yu, W. Ma and Q. Peng, *Adv. Mater.*, 2022, **34**, 2109516.

24 W. Gao, F. Qi, Z. Peng, F. R. Lin, K. Jiang, C. Zhong, W. Kaminsky, Z. Guan, C.-S. Lee, T. J. Marks, H. Ade and A. K.-Y. Jen, *Adv. Mater.*, 2022, **34**, 2202089.

25 R. Sun, Y. Wu, X. Yang, Y. Gao, Z. Chen, K. Li, J. Qiao, T. Wang, J. Guo, C. Liu, X. Hao, H. Zhu and J. Min, *Adv. Mater.*, 2022, **34**, 2110147.

26 Y. Wei, Z. Chen, G. Lu, N. Yu, C. Li, J. Gao, X. Gu, X. Hao, G. Lu, Z. Tang, J. Zhang, Z. Wei, X. Zhang and H. Huang, *Adv. Mater.*, 2022, **34**, 2204718.

27 L. Zhu, M. Zhang, J. Xu, C. Li, J. Yan, G. Zhou, W. Zhong, T. Hao, J. Song, X. Xue, Z. Zhou, R. Zeng, H. Zhu, C.-C. Chen, R. C. I. MacKenzie, Y. Zou, J. Nelson, Y. Zhang, Y. Sun and F. Liu, *Nat. Mater.*, 2022, **21**, 656–663.

28 Q. Liu, Y. Jiang, K. Jin, J. Qin, J. Xu, W. Li, J. Xiong, J. Liu, Z. Xiao, K. Sun, S. Yang, X. Zhang and L. Ding, *Sci. Bull.*, 2020, **65**, 272–275.

29 J. Qin, L. Zhang, C. Zuo, Z. Xiao, Y. Yuan, S. Yang, F. Hao, M. Cheng, K. Sun, Q. Bao, Z. Bin, Z. Jin and L. Ding, *J. Semicond.*, 2021, **42**, 010501.

30 P. Li, X. Meng, K. Jin, Z. Xu, J. Zhang, L. Zhang, C. Niu, F. Tan, C. Yi, Z. Xiao, Y. Feng, G.-W. Wang and L. Ding, *Carbon Energy*, 2023, **5**, e250.

31 D. H. Shin and S.-H. Choi, *Coatings*, 2018, **8**, 329.

32 P. Yin, Z. Yin, Y. Ma and Q. Zheng, *Energy Environ. Sci.*, 2020, **13**, 5177–5185.

33 H.-W. Cheng, Y. Zhao and Y. Yang, *Adv. Energy Mater.*, 2022, **12**, 2102908.

34 C.-C. Chen, L. Dou, R. Zhu, C.-H. Chung, T.-B. Song, Y. B. Zheng, S. Hawks, G. Li, P. S. Weiss and Y. Yang, *ACS Nano*, 2012, **6**, 7185–7190.

35 L. Dou, J. You, J. Yang, C.-C. Chen, Y. He, S. Murase, T. Moriarty, K. Emery, G. Li and Y. Yang, *Nat. Photonics*, 2012, **6**, 180–185.

36 C.-C. Chueh, S.-C. Chien, H.-L. Yip, J. F. Salinas, C.-Z. Li, K.-S. Chen, F.-C. Chen, W.-C. Chen and A. K.-Y. Jen, *Adv. Energy Mater.*, 2013, **3**, 417–423.

37 C.-Y. Chang, L. Zuo, H.-L. Yip, Y. Li, C.-Z. Li, C.-S. Hsu, Y.-J. Cheng, H. Chen and A. K.-Y. Jen, *Adv. Funct. Mater.*, 2013, **23**, 5084–5090.

38 L. Dou, C.-C. Chen, K. Yoshimura, K. Ohya, W.-H. Chang, J. Gao, Y. Liu, E. Richard and Y. Yang, *Macromolecules*, 2013, **46**, 3384–3390.

39 Y. Xie, R. Xia, T. Li, L. Ye, X. Zhan, H.-L. Yip and Y. Sun, *Small Methods*, 2019, **3**, 1900424.

40 S.-H. Liao, H.-J. Jhuo, Y.-S. Cheng and S.-A. Chen, *Adv. Mater.*, 2013, **25**, 4766–4771.

41 H. Yao, L. Ye, H. Zhang, S. Li, S. Zhang and J. Hou, *Chem. Rev.*, 2016, **116**, 7397–7457.

42 X. Ma, Z. Xiao, Q. An, M. Zhang, Z. Hu, J. Wang, L. Ding and F. Zhang, *J. Mater. Chem. A*, 2018, **6**, 21485–21492.

43 W. Liu, S. Sun, S. Xu, H. Zhang, Y. Zheng, Z. Wei and X. Zhu, *Adv. Mater.*, 2022, **34**, 2200337.

44 Y. Li, X. Guo, Z. Peng, B. Qu, H. Yan, H. Ade, M. Zhang and S. R. Forrest, *Proc. Natl. Acad. Sci. U. S. A.*, 2020, **117**, 21147–21154.

45 X. Huang, Y. Cheng, Y. Fang, L. Zhang, X. Hu, S. Y. Jeong, H. Zhang, H. Y. Woo, F. Wu and L. Chen, *Energy Environ. Sci.*, 2022, **15**, 4776–4788.

46 M. Zhang, X. Guo, W. Ma, H. Ade and J. Hou, *Adv. Mater.*, 2015, **27**, 4655–4660.

47 J. Jing, S. Dong, K. Zhang, Z. Zhou, Q. Xue, Y. Song, Z. Du, M. Ren and F. Huang, *Adv. Energy Mater.*, 2022, **12**, 2200453.

48 S. Guan, Y. Li, K. Yan, W. Fu, L. Zuo and H. Chen, *Adv. Mater.*, 2022, **34**, 2205844.

49 X. Liu, Z. Zhong, R. Zhu, J. Yu and G. Li, *Joule*, 2022, **6**, 1918–1930.

50 J. Liu, L. Liu, C. Zuo, Z. Xiao, Y. Zou, Z. Jin and L. Ding, *Sci. Bull.*, 2019, **64**, 1655–1657.

51 J. Xiong, K. Jin, Y. Jiang, J. Qin, T. Wang, J. Liu, Q. Liu, H. Peng, X. Li, A. Sun, X. Meng, L. Zhang, L. Liu, W. Li, Z. Fang, X. Jia, Z. Xiao, Y. Feng, X. Zhang, K. Sun, S. Yang, S. Shi and L. Ding, *Sci. Bull.*, 2019, **64**, 1573–1576.

52 J. Xiong, J. Xu, Y. Jiang, Z. Xiao, Q. Bao, F. Hao, Y. Feng, B. Zhang, Z. Jin and L. Ding, *Sci. Bull.*, 2020, **65**, 1792–1795.

53 Y. Jiang, K. Jin, X. Chen, Z. Xiao, X. Zhang and L. Ding, *J. Semicond.*, 2021, **42**, 070501.

54 X. Chen, Y. Luo, M. Lv, C. Yi, M. Yin, S. Liu, Z. Xiao and L. Ding, *Mater. Chem. Front.*, 2022, **6**, 802–806.

55 K. Jin, Z. Ou, L. Zhang, Y. Yuan, Z. Xiao, Q. Song, C. Yi and L. Ding, *J. Semicond.*, 2022, **43**, 050501.

56 Z. Ou, J. Qin, K. Jin, J. Zhang, L. Zhang, C. Yi, Z. Jin, Q. Song, K. Sun, J. Yang, Z. Xiao and L. Ding, *J. Mater. Chem. A*, 2022, **10**, 3314–3320.

57 G. Zong, M. Li, K. Jin, Z. Xu, L. Zhang, N. Ma, J. Wang, G.-W. Wang, Z. Xiao and L. Ding, *Mater. Chem. Front.*, 2022, **6**, 1858–1864.

58 K. Jiang, Q. Wei, J. Y. L. Lai, Z. Peng, H. K. Kim, J. Yuan, L. Ye, H. Ade, Y. Zou and H. Yan, *Joule*, 2019, **3**, 3020–3033.

59 W. Yang, W. Wang, Y. Wang, R. Sun, J. Guo, H. Li, M. Shi, J. Guo, Y. Wu, T. Wang, G. Lu, C. J. Brabec, Y. Li and J. Min, *Joule*, 2021, **5**, 1209.

60 R. Po, G. Bianchi, C. Carbonera and A. Pellegrino, *Macromolecules*, 2015, **48**, 453.

61 Z. Chiguvare and V. Dyakonov, *Phys. Rev. B: Condens. Matter Mater. Phys.*, 2004, **70**, 235207.

62 Y. Rui, Z. Jin, X. Fan, W. Li, B. Li, T. Li, Y. Wang, L. Wang and J. Liang, *Mater. Futures*, 2022, **1**, 045101.

63 J. Wang, D. Li, J. Wang and J. Peng, *Mater. Futures*, 2022, **1**, 045301.

64 X. Meng, M. Li, K. Jin, L. Zhang, J. Sun, W. Zhang, C. Yi, J. Yang, F. Hao, G.-W. Wang, Z. Xiao and L. Ding, *Angew. Chem., Int. Ed.*, 2022, **61**, e202207762.

65 Z. Hu, Z. Wang and F. Zhang, *J. Mater. Chem. A*, 2019, **7**, 7025–7032.

66 N. Schopp, G. Akhtanova, P. Panoy, A. Arbuz, S. Chae, A. Yi, H. J. Kim, V. Promarak, T.-Q. Nguyen and V. V. Brus, *Adv. Mater.*, 2022, **34**, 2203796.

67 R. Xu, J. Guo, S. Mi, H. Wen, F. Pang, W. Ji and Z. Cheng, *Mater. Futures*, 2022, **1**, 032302.

68 C. Xu, K. Jin, Z. Xiao, Z. Zhao, X. Ma, X. Wang, J. Li, W. Xu, S. Zhang, L. Ding and F. Zhang, *Adv. Funct. Mater.*, 2021, **31**, 2107934.

69 Z. Wen, T. Wang, Z. Chen, T. Jiang, L. Feng, X. Feng, C. Qin and X. Hao, *Chin. Chem. Lett.*, 2021, **32**, 529–534.

70 G. Chai, Y. Chang, J. Zhang, X. Xu, L. Yu, X. Zou, X. Li, Y. Chen, S. Luo, B. Liu, F. Bai, Z. Luo, H. Yu, J. Liang, T. Liu, K. S. Wong, H. Zhou, Q. Peng and H. Yan, *Energy Environ. Sci.*, 2021, **14**, 3469–3479.

71 A. Shang, S. Luo, J. Zhang, H. Zhao, X. Xia, M. Pan, C. Li, Y. Chen, J. Yi, X. Lu, W. Ma, H. Yan and H. Hu, *Sci. China: Chem.*, 2022, **65**, 1758–1766.

72 Z. Hu, J. Wang, X. Ma, J. Gao, C. Xu, K. Yang, Z. Wang, J. Zhang and F. Zhang, *Nano Energy*, 2020, **78**, 105376.

73 L. Vitos, A. V. Ruban, H. L. Skriver and J. Kollár, *Surf. Sci.*, 1998, **411**, 186–202.

74 S. Schubert, J. Meiss, L. Müller-Meskamp and K. Leo, *Adv. Energy Mater.*, 2013, **3**, 438–443.

75 X. Huang, L. Zhang, Y. Cheng, J. Oh, C. Li, B. Huang, L. Zhao, J. Deng, Y. Zhang, Z. Liu, F. Wu, X. Hu, C. Yang, L. Chen and Y. Chen, *Adv. Funct. Mater.*, 2021, **32**, 2108634.

76 A. Colsmann, A. Puetz, A. Bauer, J. Hanisch, E. Ahlswede and U. Lemmer, *Adv. Energy Mater.*, 2011, **1**, 599.

77 G. Xu, L. Shen, C. Cui, S. Wen, R. Xue, W. Chen, H. Chen, J. Zhang, H. Li, Y. Li and Y. Li, *Adv. Funct. Mater.*, 2017, **27**, 1605908.

78 J. Zhang, G. Xu, F. Tao, G. Zeng, M. Zhang, Y. Yang, Y. Li and Y. Li, *Adv. Mater.*, 2019, **31**, 1807159.